



## REVIEW ARTICLE

# Synergistic removal of mixed methyl orange/sunset yellow solution by the graded ZnCrNi-LDHs porous material



Li Yang<sup>a,1</sup>, Tian Huiyuan<sup>a,1</sup>, Xia Mengyan<sup>a</sup>, Cui Baoyu<sup>a</sup>, Liu Chang<sup>a</sup>,  
Du Xiuhong<sup>c</sup>, Wang Zehua<sup>a</sup>, Duan Xianying<sup>d,e,\*</sup>, Cui Jiehu<sup>a,b,\*</sup>

<sup>a</sup> School of Materials science and Engineering, Zhengzhou University of Aeronautics, Zhengzhou, PR China

<sup>b</sup> Henan Engineering Research Center for Ceramic Materials Interface, Zhengzhou University of Aeronautics, Zhengzhou, PR China

<sup>c</sup> Clinical Laboratory Medicine, Henan Medical College, Zhengzhou, PR China

<sup>d</sup> School of Medicine, Huanghe Science and Technology University, Zhengzhou, PR China

<sup>e</sup> Institute of Chemistry, Henan Academy of Sciences, Zhengzhou, Henan 450002, PR China

Received 16 March 2023; accepted 9 July 2023

Available online 13 July 2023

## KEYWORDS

ZnCrNi-LDHs-like hydro-  
talcite;  
Mixed adsorption;  
Anionic dyes;  
Water treatment;  
Graded porous

**Abstract** Layered bimetallic hydroxide (LDHs) nanomaterials have shown excellent potential in the field of recovery of pollutants from wastewater through anion exchange and surface electrostatic interaction. In this paper, three new ternary ZnCrNi-LDHs with the different graded porous were successfully prepared by controlling the morphology of the layer stacking using triethanolamine as the soft-template, and characterized by SEM, TEM, XPS, TG, BET and XRD. The ZnCrNi-LDHs exhibited higher adsorption capacity for pollutants such as methyl orange, sunset yellow and their mixed solutions. The results showed that there was a good synergistic adsorption effect in the adsorption process of mixed solutions. The maximum adsorption amounts of single methyl orange, sunset yellow, and mixed solutions of methyl orange and sunset yellow were 1834.63 mg·g<sup>-1</sup>, 1259.79 mg·g<sup>-1</sup>, 3270.59 mg·g<sup>-1</sup> and 3294.38 mg·g<sup>-1</sup>, which shows that the adsorption amounts about synergistic adsorption effect for mixed solutions is much higher than those of single methyl orange and sunset yellow; Meanwhile, the maximum adsorption capacity is higher than most adsorbents. The pseudo-second-order kinetic model fitted the kinetic data of adsorption, while the equilibrium adsorption isotherm data followed the Freundlich model. The adsorption process contains both surface adsorption and interlayer anion exchange as determined by SEM, XRD, IR and zeta

\* Corresponding author.

E-mail addresses: [dxynumber@163.com](mailto:dxynumber@163.com) (D. Xianying), [cuijiehu@163.com](mailto:cuijiehu@163.com) (C. Jiehu).

<sup>1</sup> These authors contributed equally to this work.

Peer review under responsibility of King Saud University.



potential analysis. The research not only demonstrates that three ZnCrNi-LDHs materials showed excellent adsorption performance and practical interest as an efficient adsorbent for the removal of methyl orange, sunset yellow, and mixed solutions but also provides a strategy for the removal of mixed dye solutions.

© 2023 The Author(s). Published by Elsevier B.V. on behalf of King Saud University. This is an open access article under the CC BY-NC-ND license (<http://creativecommons.org/licenses/by-nc-nd/4.0/>).

## 1. Introduction

Dye wastewater is one of the main industrial wastewaters that contain a large number of different dyes, and the water environmental safety caused by dye wastewater has become one of the most challenging environmental problems in current society (Chen et al., 2021). In particular, azo dyes such as Methyl orange (MO) and sunset yellow (SY) are the most typical anionic dyes, which have caused serious ecological problems due to their toxicity, carcinogenicity, and teratogenicity (Grover et al., 2022). The adsorption technique has received extensive research because of its simple operation, high removal rate, fast adsorption rate, and lack of secondary pollution for organic dye removal from wastewaters (Chen et al., 2019). A large number of adsorption articles have been reported about the adsorption properties of single MO and SY wastewaters. In recent years, LDH has been widely studied as a multi-functional environmental protection material with low cost, a large specific surface area, and stable performance (Hucheng et al., 2022). Zili Jiang et al (Jiang et al., 2022) achieved a maximum adsorption capacity of 806 mg·g<sup>-1</sup> of MO using Ni/Cr LDH as adsorbent by co-precipitation; Lin Jia et al (Lin et al., 2022) prepared a photo catalytically regenerated ZnCr-CO<sub>3</sub><sup>2-</sup> LDH using co-precipitation, and the maximum adsorption of MO at 25 °C and pH = 3 was 938.08 mg·g<sup>-1</sup>; M. Ghaedi et al (Ghaedi et al., 2015) used new adsorptive gold nanoparticles (Au-NP-AC) loaded on activated carbon to adsorb MO and SY with the maximum adsorption of 161.29 mg·g<sup>-1</sup>, 227.27 mg·g<sup>-1</sup>, and F. Ghaedi (Xu et al., 2017) used a new gold nanoparticle (Au-NP-AC) loaded on activated carbon to adsorb MO; Reda M. Abdelhameed et al (Reda M. Abdelhameed et al., 2021) prepared three phthalocyanines (Pcs) derivatives with Al<sup>3+</sup> and Co<sup>2+</sup> ions as the central metal attached to MOF substrates and studied the photocatalytic decay performance of methylene blue (MB) and methyl orange (MO) and their mixtures under visible light irradiation, and the degradation rates of the three catalysts reached 0.012, 0.035, and 0.046 min<sup>-1</sup> for MB and 0.027, 0.052, and 0.082 min<sup>-1</sup> for MO. The high performance of the porous MOF materials prepared in the literature not only as carriers but also as electron acceptors enhance photostability and photocatalytic activity. Up to now, a large number of studies have reported that single dye waste waters were removed using a single adsorbent (Lei et al., 2017); however, there is little research on the treatment of different dye wastewaters with one adsorbent at the same time due to the effect on different molecule sizes and properties of dye molecules, so it is a challenge to remove MO and SY using one single adsorbent with high capacity. Therefore, it is crucial to design a highly efficient, inexpensive, and stable adsorbent with a high capacity for mixed dye wastewaters adsorption separation.

Layered double hydroxides (LDHs) with anion exchange ability are often selected as an efficient adsorbing material for selectively removing of anionic dye (Jie et al., 2022). Now, more and more research is focused on the expansion of binary metal LDH to ternary metal and even quaternary metal LDH by cation doping for higher adsorption performance (Wang et al., 2022). The ternary metal LDH materials have also gradually become a research hotspot for researchers (Dong et al., 2017). Although there are studies on the removal of single-dye wastewater, few researchers have conducted detailed studies on mixed-dye wastewater using LDHs as adsorbents. This prompted us to explore the adsorption separation of mixed dye wastewater by ternary LDH materials. The synthesis process of LDH requires constant or variable pH conditions. Urea, sodium hydroxide and triethanolamine

can be commonly used. Triethanolamine acts as a soft templating agent show its advantage which slowly releases OH<sup>-</sup> when performing hydrothermal synthesis in order to synthesizes a more uniform lamellar form of LDH.

According to the IUPAC definition (Song et al., 2018), pore sizes with less than 2 nm, 2–50 nm and larger than 50 nm are microporous materials, mesoporous or mesoporous and macroporous, respectively. Graded porous materials refer to porous materials containing two or more types of porosity (Cheng, 2012). The porosity presence of micropores and mesopores materials will help to enhance the selectivity effect of the size and shape of the guest molecules (Sun et al., 2016); and the presence of macropores also reduce the diffusion resistance which facilitates the transport of reactant and product molecules (Zheng et al., 2018) so that the pore structures of different sizes have synergistic effects. The preparation methods of graded porous materials include hard template, soft template, no template, biotemplate (Abdelfattah et al., 2022), and post-process etching (Zheng, 2019).

Based on the above discussion, in this paper, we designed and prepared three new graded porous ternary ZnCrNi-LDHs graded porous adsorbents by our group's Triethanolamine (TEA)-assisted hydrothermal method. They were characterized by SEM, EDS, XRD, IR, XPS, TG, and other characterization analyses. The adsorption effect of three ZnCrNi-LDHs from waste-water treatment were studied using anionic dyes MO, SY and their mixed solutions as pollutants. The mutual influence of adsorbents on the adsorption process of mixed anionic dye wastewaters such as pH, adsorbent dosage and other factors, the adsorption mechanism and their adsorption performance were studied. They will lay the foundation for the practical treatment of adsorbents in dye wastewaters (Zhang, 2019). The adsorption kinetics, equilibrium and mechanism were also discussed.

## 2. Experimental section

### 2.1. Materials

Zn(NO<sub>3</sub>)<sub>2</sub>·6H<sub>2</sub>O, Cr(NO<sub>3</sub>)<sub>3</sub>·9H<sub>2</sub>O, Ni(NO<sub>3</sub>)<sub>2</sub>·6H<sub>2</sub>O, triethanolamine(C<sub>6</sub>H<sub>15</sub>NO<sub>3</sub>), sunset yellow (C<sub>16</sub>H<sub>10</sub>N<sub>2</sub>Na<sub>2</sub>O<sub>7</sub>S<sub>2</sub>, abbreviated here as SY), etc. were purchased from Tianjin Comio Chemical Reagent Co. Methyl orange(C<sub>14</sub>H<sub>14</sub>N<sub>3</sub>O<sub>3</sub>-SNa, here abbreviated as MO) was purchased from Luoyang Chemical Reagent Factory; anhydrous ethanol (C<sub>2</sub>H<sub>6</sub>O) was purchased from Zhengzhou Pini Chemical Reagent Factory; all the above reagents were analytically pure. The water used in the laboratory was all deionized water.

### 2.2. Preparation of ZnCrNi-LDHs

In this study, ZnCrNi-LDHs nanomaterials were prepared by hydrothermal method. The mixture of zinc nitrate hexahydrate, chromium nitrate nonahydrate and nickel nitrate hexahydrate was weighed in the molar ratio of 1:1:1 to a total of 0.01mol in a beaker, then 12 mL of water was added and stirred on a magnetic stirrer, and when it was stirred well 2 mL of triethanolamine solution was added drop by drop. The mixture was stirred for 5 min and poured into the auto-

clave liner; the reactor was transferred to a blast drying oven, and the reaction time was set at 110 °C and the temperature was set at 3 h. After the reaction was completed. The obtained precipitate was centrifuged, washed with water and ethanol and repeated three times, and the precipitate was dried in a vacuum drying oven at 60 °C. The light purple powder obtained by grinding and named as ZnCrNi-LDHs-2, ZnCrNi-LDHs-3, ZnCrNi-LDHs-4 based on quantity of triethanolamine (2, 3 and 4 mL), respectively.

### 2.3. Characterization

The ZnCrNi-LDHs were characterized using scanning electron microscopy (SEM), X-ray diffractogram (XRD), Fourier transform infrared spectroscopy (FTIR), Brunauer-Emmett-Teller (BET), X-ray photoelectron spectroscopy (XPS), Inductively Coupled Plasma-Optical Emission Spectroscopy (ICP-OES) and thermogravimetry (TG). A Bruker D8ANCE X-ray diffraction analyzer from Bruker, Germany was used with a Cu-K $\alpha$  target ( $\lambda = 1.5418 \text{ \AA}$ ), a scanning speed of 8°/min from 5° to 70° and an operating voltage and current of 40 kV and 30 mA, respectively. microscopic morphology was observed with a Vega 3 Tescan SEM at an accelerating voltage of 20.0 kV. The spectral range of 500–4000 cm<sup>-1</sup> was determined using dried KBr pellets on a NICOLET VERTEX 70-V spectrometer. nitrogen adsorption-desorption isotherms were determined using a Micromeritics ASAP 2000 analyzer. X-ray photoelectron spectroscopy was completed with an ESCALAB 250Xi. The ICP (iCAP 7200 ICP-OES, Thermo Fisher Scientific-US) light source has a frequency of 40.68 MHz and a power of 0.8–1.5 kW. TG was characterized on a Perkin-Elmer thermogravimetric analyzer Pyris 1 TGA up to 1023 K using a heating rate of 10 K min<sup>-1</sup> under N<sub>2</sub> atmosphere.

### 2.4. Adsorption experiments

25 mg ZnCrNi-LDHs adsorbent was added to 20 mL of MO/SY and mixed solution at a concentration of 500 mg/L. The mixture was placed on a stirrer at constant pH at room temperature for 1 h to reach adsorption equilibrium. After adsorption, the adsorbent was centrifuged and the concentration of dye at equilibrium was measured at 464 nm (MO) and 482 nm (SY) using a UV spectrophotometer, and the adsorption and removal rates of the adsorbent on MO, SY and their mixed solutions were calculated respectively.

$$\text{Adsorption amount} : Q_e = \frac{(C_0 - C_e) \times V}{m}$$

$$\text{Removal rate} : R = \frac{C_0 - C_e}{C_0} \times 100\%$$

In this equation:  $C_0$ - the initial concentration of the dye wastewaters, mg/L;  $C_e$ - the concentration of the dye wastewaters after adsorption equilibrium, mg/L;  $V$ - the volume of dye wastewaters, L;  $m$ - the amount of adsorbent, g.

## 3. Results and discussion

### 3.1. Characterization

SEM images of ZnCrNi-LDHs with three different triethanolamine additions are presented in Fig. 1 (a-c). As shown

in Fig. 1 (a-c), all three materials are formed by the stacking of irregular nanosheets which are stacked by face-to-face contact and eventually stacked into a 3D porous structure. Those structures can create more intercalated structures which allows more nitrate ions/water molecules to enter into the interlayer space (Lin J, 2021), thus further improving the ion exchange capacity of ZnCrNi-LDHs, and it also forms the pore sizes of different sizes which is more conducive to the transport of ion exchange. It can be seen that the thickness of the LDHs nanosheets gradually becomes thinner, and more interlayer structures are stacked, providing an increase in the adsorption sites from ZnCrNi-LDHs-2 to ZnCrNi-LDHs-4 (W et al., 2022). From the above discussion, it can be seen that the amount of triethanolamine addition can disperse the LDHs nanosheets to storm more adsorption sites. The mapping plots of EDS in Fig. 1 (d) show the coexistence of Zn, Cr, Ni, C, N and O elements in the materials (Chen et al., 2022), thus further confirming the successful preparation of ZnCrNi-LDHs-4 nanocomposites. TEM images in Fig. 1 (e-g) shows laminar structure. With the increase of triethanolamine, the lamellae become thinner, which corresponds to SEM. It proves that triethanolamine has a modulating effect on the morphology.

The XRD patterns of the ZnCrNi-LDHs nanocomposites are shown in Fig. 2(a). From Fig. 2(a), it can be seen that the ZnCrNi-LDHs have a series of characteristic diffraction peaks of well-crystallized hydrotalcite-like LDHs indexed as 003, 006, 009 and 110 located at 10.28, 20.13, 34.27 and 60.16° (Lv et al., 2020), which are consistent with the characteristics of the ZnCr-like hydrotalcite and NiCr-like hydrotalcite (Shan et al., 2012), demonstrating that three ZnCrNi-LDHs samples were successfully prepared. According to the Bragg equation ( $n\lambda = 2d \cdot \sin(\theta)$ ), the  $d$ -values of  $c$ -axis for three ZnCrNi-LDHs based on the low  $2\theta$  angle at 10.28°, 10.20° and 10.28° are minor different (8.60, 8.67 and 8.60 Å, respectively), which is consistent with the results of SEM. Meanwhile, with the increase of the addition of triethanolamine, the characteristic diffraction peak half-peak width did not change, while the peak intensity became higher and the peak shape was flat, indicating that the crystallinity of the samples changed from poor to good from ZnCrNi-LDHs-2 to ZnCrNi-LDHs-4 (Mitani et al., 2017).

The functional groups and chemical bonds in ZnCrNi-LDHs were further analyzed for investigating the chemical structures by Fourier transform infrared spectroscopy (FTIR). As shown in Fig. 2(b), it can be observed that the stretching vibration at 3415 cm<sup>-1</sup> were attributed to OH group hydrogen band stretching vibrations and hydrogen bonded to nitrate group stretching vibrations in the hydroxide layers (Chen et al., 2013). The vibration absorbance peak at 1639 cm<sup>-1</sup> is assigned to the interlayer water molecules. The vibration absorbance band at 1390 cm<sup>-1</sup> is associated with the asymmetric vibration of the interlayer NO<sub>3</sub><sup>-</sup>. The vibration absorbance peak at 1057 cm<sup>-1</sup> and 564 cm<sup>-1</sup> are the stretching vibration of the M–O and of O–M–O bond (Duan et al., 2010; Shoaib et al., 2016); including O–Zn–O bond, O–Cr–O bond and O–Ni–O bond, respectively. The small peaks below 3000 cm<sup>-1</sup> are the stretching vibrations of –CH<sub>3</sub> and –CH<sub>2</sub> groups. From the above analysis, it is evident that the LDHs have typical hydrotalcite-like peaks and the NO<sub>3</sub><sup>-</sup> groups are successfully intercalated into the hydrotalcite-like layers (Cui et al., 2020).

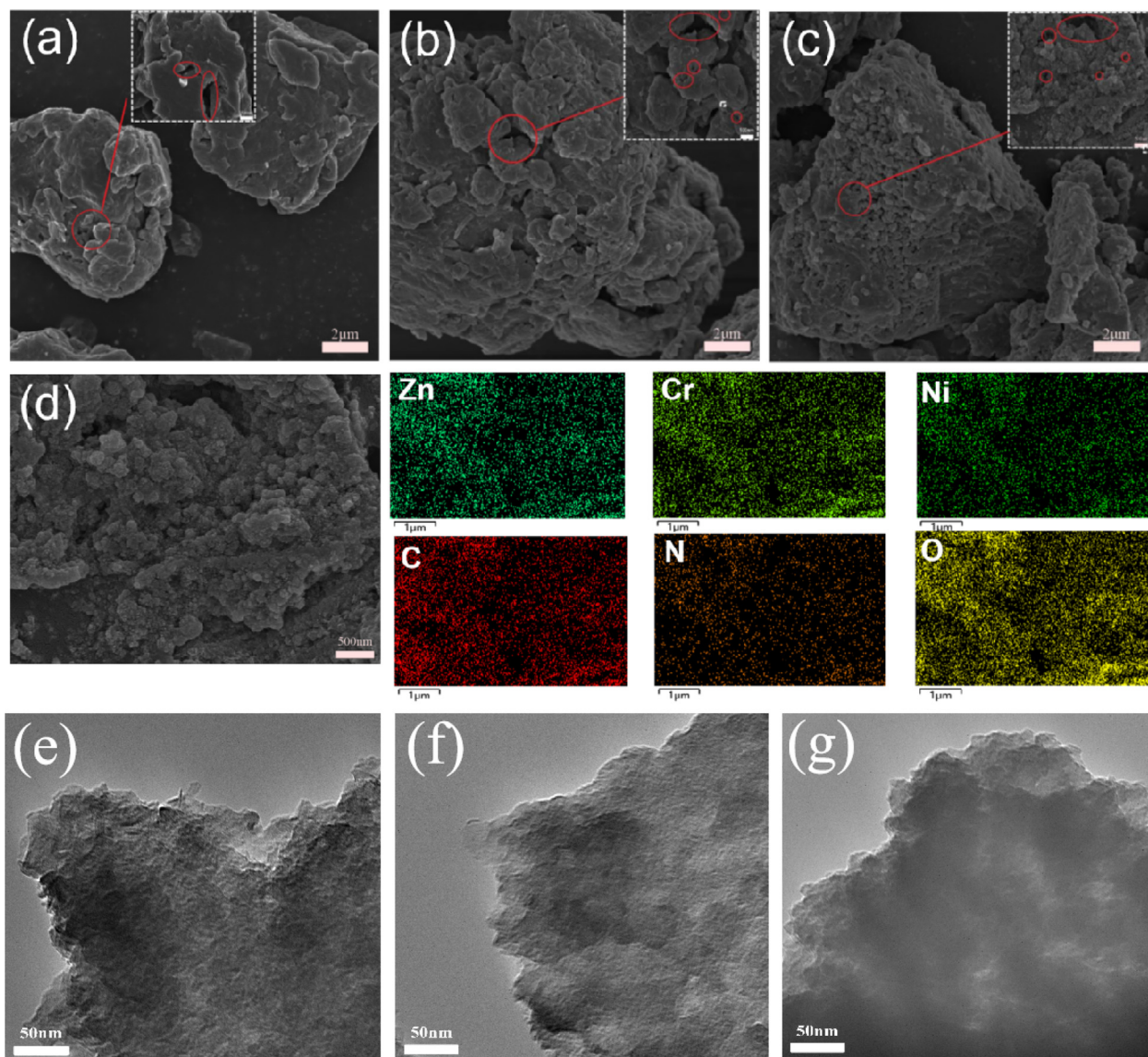


**Fig. 1** SEM images (a-c) of the three ZnCrNi-LDHs, EDS (d) of the ZnCrNi-LDHs-4 and TEM images (e-g) of the three ZnCrNi-LDHs.

The  $N_2$  adsorption–desorption isotherms and pore size distributions of ZnCrNi-LDHs are shown in Fig. 2(c-d). The  $N_2$  adsorption–desorption curves of ZnCrNi-LDHs-2, ZnCrNi-LDHs-3 and ZnCrNi-LDHs-4 all conform to type III isotherms with H4-type hysteresis loops based on the IUPAC classification in the range of from 0.1 to 1.00P/P<sub>0</sub> for ZnCrNi-LDHs-2 and ZnCrNi-LDHs-3, 0.6–1.00P/P<sub>0</sub> for ZnCrNi-LDHs-4, reflecting the results of harmonic multilayer adsorption on the surface of ZnCrNi-LDHs (Ji et al., 2009). The isotherms of all three samples with H3-type hysteresis loops indicated that three ZnCrNi-LDHs had mesoporous structures which might be related to the inhomogeneous pore sizes generated by the aggregation of the lamellar LDH structures as reported previously and more favorable to the ion exchange process of the anionic contaminants for MO and SY. The BET surface area of three Zn-Co-Ni-LDHs are 2.3578, 2.9969 and 6.0771 m<sup>2</sup>·g<sup>-1</sup>, and the relatively low speci-

fic surface area is connected with stacked 3D compact structure.

The pore size distribution diagram (Fig. 2(d)) shows the different pore sizes of three ZnCrNi-LDHs, including small mesopores, large mesopores and large pores, and the pore volumes are 0.008476, 0.010925 and 0.018017 cm<sup>3</sup>·g, and the pore diameter are 38.826, 52.533 and 122.394 nm, respectively. The larger pore sizes are likely to be large pores formed between the stacked nanosheets, while the smaller mesopores are mainly related to the pores present within the nanosheets (Sun, 2015), further confirming the synthesis of graded porous nano-like hydroxide.

The thermogravimetric-differential scanning volume technique (TG-DSC) was used to analyze the thermally stable phenotypes of materials. As shown in Fig. 2(e), it can be seen that there are two stages of weight loss in three ZnCrNi-LDHs, the first weight loss stage occurs ranging from 20 to 120 °C which

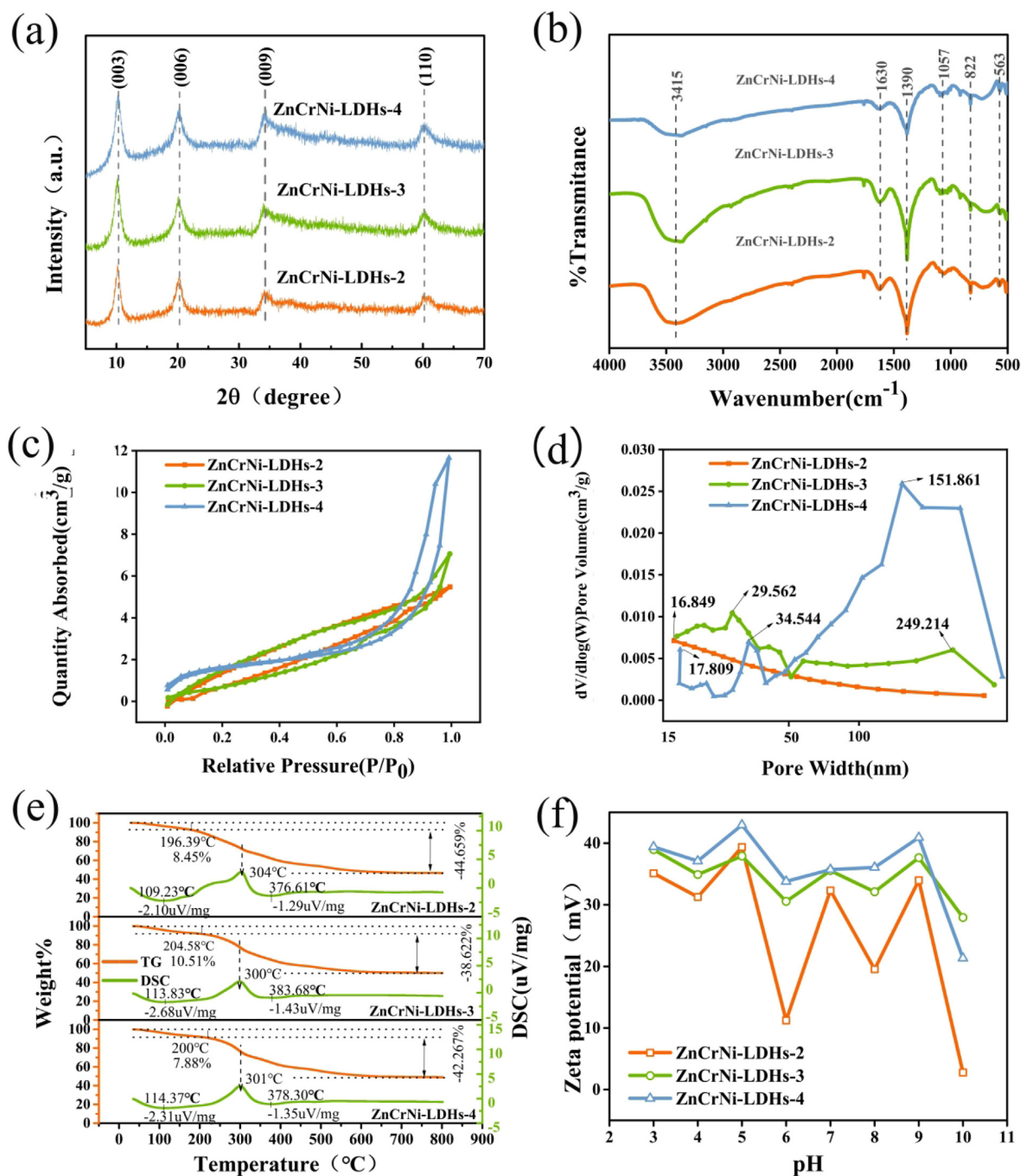


**Fig. 2** XRD patterns of ZnCrNi-LDHs (a), FTIR patterns of ZnCrNi-LDHs (b),  $N_2$  adsorption and desorption curves of ZnCrNi-LDHs (c), the pore size distribution of ZnCrNi-LDHs (d), TG-DSC patterns of ZnCrNi-LDHs (e), the zeta potential of ZnCrNi-LDHs (f).

is due to the volatilization of surface water molecules and crystalline water molecules (Zhang et al., 2021); and the weight loss accounts for 8.45%, 10.51% and 7.88% of the total mass of the samples, respectively. The second stage undergoes a heat release in the range of 120–600 °C, indicating the destruction of three ZnCrNi-LDHs layers structure and further phase transformation from hydroxides (LDHs) to oxides (LDO) at 304 °C, 300 °C and 301 °C, respectively, and this result is mainly due to the loss of nitrate ions, hydroxyl groups and tri-

ethanolamine among the layers with a weight loss of 44.659%, 38.622% and 42.267% of the total mass of the sample. It can be judged by this process that under the conditions of synthesis of LDHs (110 °C, 3 h), there is no phase change process and the LDHs synthesized by the hydrothermal method is relatively stable (Zhang et al., 2014).

To understand the surface charge of ZnCrNi-LDHs, the Zeta potential analysis of ZnCrNi-LDHs was carried out. As shown in Fig. 2(f), the zeta potential value when pH value

from 4 to 9 is 31.3, 39.4, 11.23, 32.3, 19.53 and 33.96 mV for ZnCrNi-LDHs-2, 34.9, 37.9, 30.5, 35.5, 32.1 and 37.6 mV for ZnCrNi-LDHs-3, 37.1, 42.9, 33.8, 35.7, 36.1 and 40.9 mV for ZnCrNi-LDHs-4, respectively. It can be seen that the particles were positively charged within the pH range of 4–9 of the zeta potential, indicating that three ZnCrNi-LDHs will gain high adsorption capacity by the adsorbent used electrostatic interaction to produce surface adsorption on MO and SY as well as the mixed solution (Lei et al., 2016).

For To determine the molecular formula of three ZnCrNi-LDHs, Furthermore, the ratios of  $Zn^{2+}$ ,  $Cr^{3+}$  and  $Ni^{2+}$  were analyzed using ICP-OES after the samples were dissolved in concentrated  $HNO_3$ , and C, N and O elements were determined by elemental analysis (Rezvani et al., 2023). As shown in Table 1; ICP results accurately show that the Zn/Cr/Ni ratio of three ZnCrNi-LDHs. It can be seen that the addition of triethanolamine has a large influence on their elemental content of Zn, Cr and Ni based on the raw material molar ratio of 1:1:1 for three ZnCrNi-LDHs because of the changes of the pH value of the different volume ratio TEA hydrolysis. The ratio of Zn and Ni in the material gradually increases from 12.5% to 28.1%, from 8.3% to 14.2% with the addition of triethanolamine, while the doping of Cr elements relatively decreases; According to the results of adsorption performance analysis, the increase of Zn and Ni elements is more conducive to the improvement of adsorption performance. The elemental analysis clearly demonstrated that the percentage content of C, H and N per formula unit in the three nanocomposites which is consistent with the results of TG. According to ICP, elemental analysis and TG analysis, the formula of three ZnCrNi-LDHs were determined as  $[Zn_{1.51}Cr_{1.60}Ni(OH)_{9.82}] \cdot 0.19TEA \cdot 0.76 NO_3^- \cdot xH_2O$ ,  $[Zn_{1.15}Cr_{0.84}Ni(OH)_{6.82}] \cdot 0.09TEA \cdot 0.40 NO_3^- \cdot xH_2O$ ,  $[Zn_{1.16}Cr_{0.84}Ni(OH)_{6.84}] \cdot 0.10TEA \cdot 0.36 NO_3^- \cdot xH_2O$ .

XPS spectroscopy can be used to observe the surface elemental composition and bonding configuration of the ternary composites. In order to further confirm the successful preparation, the chemical status and elemental composition of three ZnCrNi-LDHs, the element chemical composition and chemical state of three ZnCrNi-LDHs were investigated by XPS spectroscopy in Fig. 3a. Fig. 3a shows the full spectrum of the sample, further indicating the presence of Zn, Cr, Ni, C, N and O elements on the surface of three ZnCrNi-LDHs with C1s at 284.8 eV originating from contaminated carbon, in agreement with the results of EDS elemental mapping. As shown in Fig. 2b, Zn 2p ( $2p_{3/2}$  and  $2p_{1/2}$ ) peaks with binding energy 1021.63 eV and 1044.69 eV for ZnCrNi-LDHs-2, 1021.64 eV and 1044.69 eV for ZnCrNi-LDHs-3 and 1021.46 eV and 1044.53 eV for ZnCrNi-LDHs-4 have the similar shape and region, revealing the similar electronic states of  $Zn^{2+}$  in three ZnCrNi-LDHs. According to previous literature, it is generally believed that Ni is in + 2 oxidation state and Cr are in + 3 oxidation states in the bimetallic NiCr LDHs. While the electronic states of Ni and Cr in the trimetallic ZnCrNi-LDHs is more intricate than in the bimetallic NiCr-LDHs. The Cr 2p spectrum is displayed in Fig. 3c. Two broad peaks for three ZnCrNi-LDHs at 586 and 577 eV correspond to the Cr  $2p_{1/2}$  and Cr  $2p_{3/2}$ , respectively. Two fitting Cr2p peaks at 577.6 and 576.2 eV can be attributed to  $Cr^{3+}-O$  and  $Cr^{3+}-OH$ , respectively (Dong et al., 2016; Zhang et al., 2023). Meanwhile, four peaks for ZnCrNi-LDHs in the Ni2p region were observed (Fig. 2(d)). The four peaks at

855.69 eV, 857.35 eV, 873.34 eV and 875.76 eV) were all fitted the characteristic peaks of the  $Ni2p_{3/2}$  and  $Ni2p_{1/2}$ , respectively, confirming that the nickel element in three ZnCrNi-LDHs exists in  $Ni^{2+}$  and  $Ni^{3+}$  state (Wang et al., 2023).

### 3.2. Adsorption behavior of ZnCrNi-LDHs on single and mixed MO/SY solutions

#### 3.2.1. Effect of adsorbent dosage and pH on the adsorption of single and mixed MO/SY solutions

Up to now, organic dyes are still one of the major classes of pollutants which are difficult to be degraded, so it is a challenge to remove methyl orange and sunset yellow from waste water. While, although many researchers have done a lot of research on single dye wastewaters, there are few studies on the removal of mixed dye wastewaters, in this paper, so single MO/SY and mixed MO/SY were chosen as the target contaminant to study the adsorption behavior of as-prepared sample ZnCrNi-LDHs-4.

Fig. 4 (a) presents the effect of adsorbent dosage from 10 to 55 mg on the adsorption performance of adsorption single dye solution and mixed dye solution. ( $0.025 \pm 0.0005$ ) g of ZnCrNi-LDHs-4 was added to 500 mg/L of MO/SY solution at the nature pH and stirred for 1 h at room temperature in a magnetic stirrer. The absorption wavelength of the solution was measured using a visible spectrophotometer after the adsorption was completed and the equilibrium adsorption amount was calculated. It can be seen from the Fig. 4 (a) that the adsorption of MO in the single solution and the adsorption of MO in the mixed solution reached the equilibrium state after 20 mg of ZnCrNi-LDHs and could reach more than 99% of the adsorption solution, and the adsorbent was extremely strong for the adsorption of MO in both the single solution and the mixed solution; While comparing to effect of the amount of adsorbent on MO, the adsorption of SY in the single solution and in the mixed solution reached the equilibrium state after 40 mg of of ZnCrNi-LDHs. The difference of the adsorption equilibrium states was probably due to the relative molecular mass of MO (327.33) molecule and molecule size was smaller compared with that of SY (452.37), so MO was more easily adsorbed to the surface or exchanged with the nitrate ions between the layers, at which time the layer spacing of the adsorbent became larger, which was consistent with the XRD characterization that the (003) characteristic peak shifted to the left, the diffraction angle became smaller from  $10.28$  to  $7.69^\circ$ , indicating the interlayer spacing became larger from 0.860 to 1.149 nm. When the effective adsorption sites were occupied after the exchange of MO with a smaller chain length, resulting in the adsorption of SY by the adsorbent is less effective than that of MO. The adsorption of SY from a mixed solution was better than that from a single solution, probably since more solutes in the mixed solution increased the concentration gradient of the solution, which promoted the adsorption of SY.

Fig. 4(b) exhibits the effect of pH on the adsorption performance of the adsorbed single solution and the mixed solution with the pH range from 4 to 9. As shown in Fig. 4(b), the adsorption of MO and SY by the adsorbent can reach more than 95% in a single solution. In the adsorption of mixed solutions, in a neutral environment, the adsorbent has the best effect on MO and SY, which can reach more than 90% for

	Zn (%)	Cr (%)	Ni (%)	C (%)	H (%)	N (%)
ZnCrNi-LDHs-2	12.5502%	13.3092%	8.3119%	9.58	3.648	6.33
ZnCrNi-LDHs-3	15.0310%	10.9477%	13.0903%	7.01	3.398	5.18
ZnCrNi-LDHs-4	16.4602%	11.9439%	14.2014%	8.39	3.501	5.13

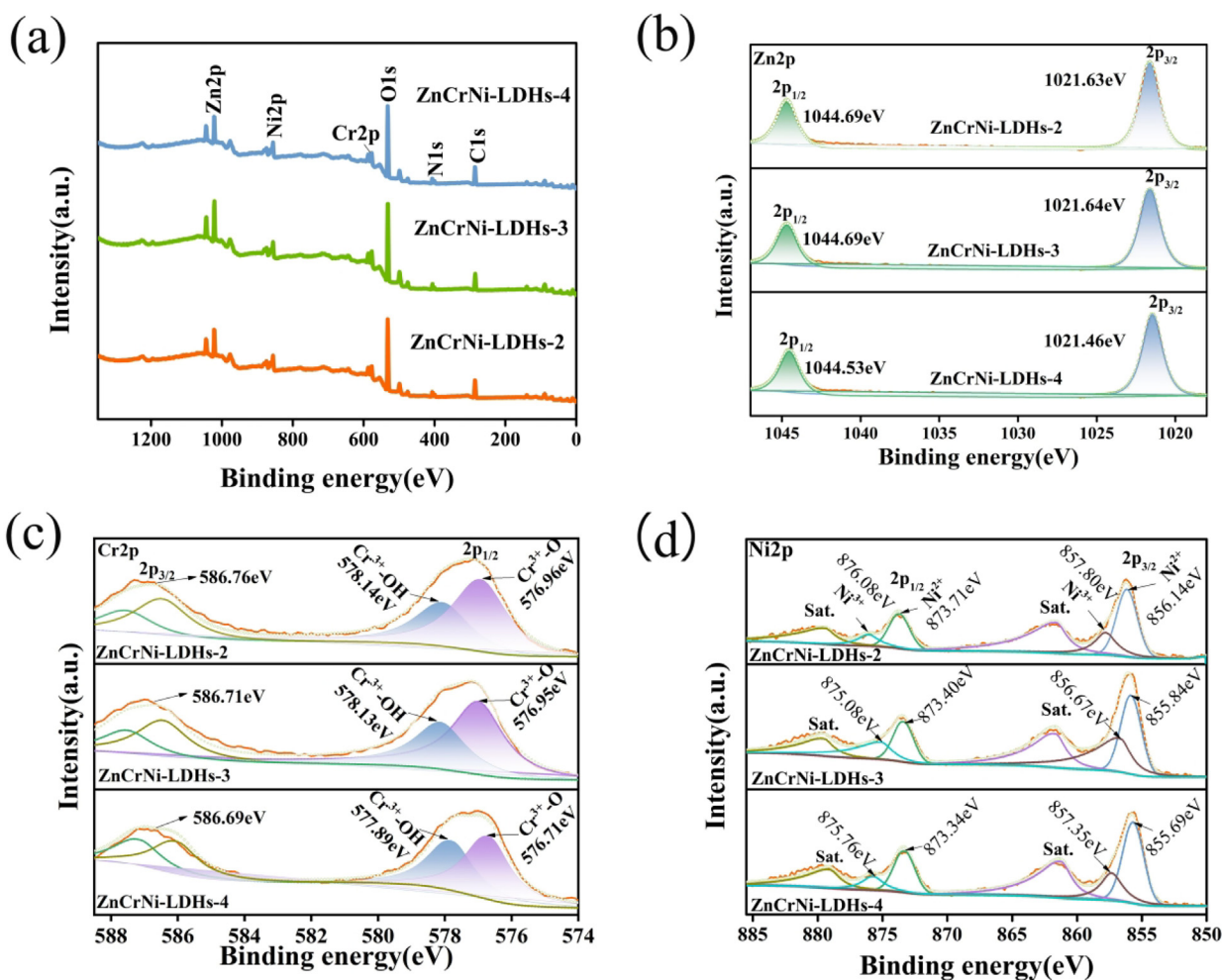


**Fig. 3** XPS survey spectra(a). High-resolution x-ray photoelectron spectra of Zn 2p regions(b),Cr 2p regions(c),Ni 2p regions(d) in three ZnCrNi-LDHs.

MO, 85% for SY, respectively. In an acidic and alkaline environment, the adsorbent can reach more than 80% on MO and more than 60% on SY. In an acidic environment, the benzene sulfonic acid group of MO and SY combines with hydroxide ion, which makes the removal rate decrease. In alkaline conditions, the hydroxide ions competed with the anions of MO and SY for adsorption, resulting in lower removal rates. The reason that the overall better adsorption effect of single solution than mixed adsorption may be that since under the condition of adsorbent quantification, the adsorption sites of the adsorbent are limited, and there are more anions in the mixed solution than in the single solution, so the adsorption effect of the single solution is better.

### 3.2.2. Effect of initial concentration and reaction time on the adsorption of MO/SY

The initial concentration is a significant effect factor in the adsorption process. The conditions of pH, adsorbent dosage, volume and stirring rate were fixed, and the initial concentration of methyl orange/sunset yellow was varied from 10 mg/L to 5000 mg/L with stirring for 1 h. The remaining concentrations of methyl orange/sunset yellow were measured separately after the adsorption was completed, and the equilibrium adsorption amount was calculated. Fig. 4 (c) demonstrates the influence of the initial concentration of the solution on the adsorption performance of the adsorbed single and mixed solutions. As shown in Fig. 4(c), the adsorption of the adsor-

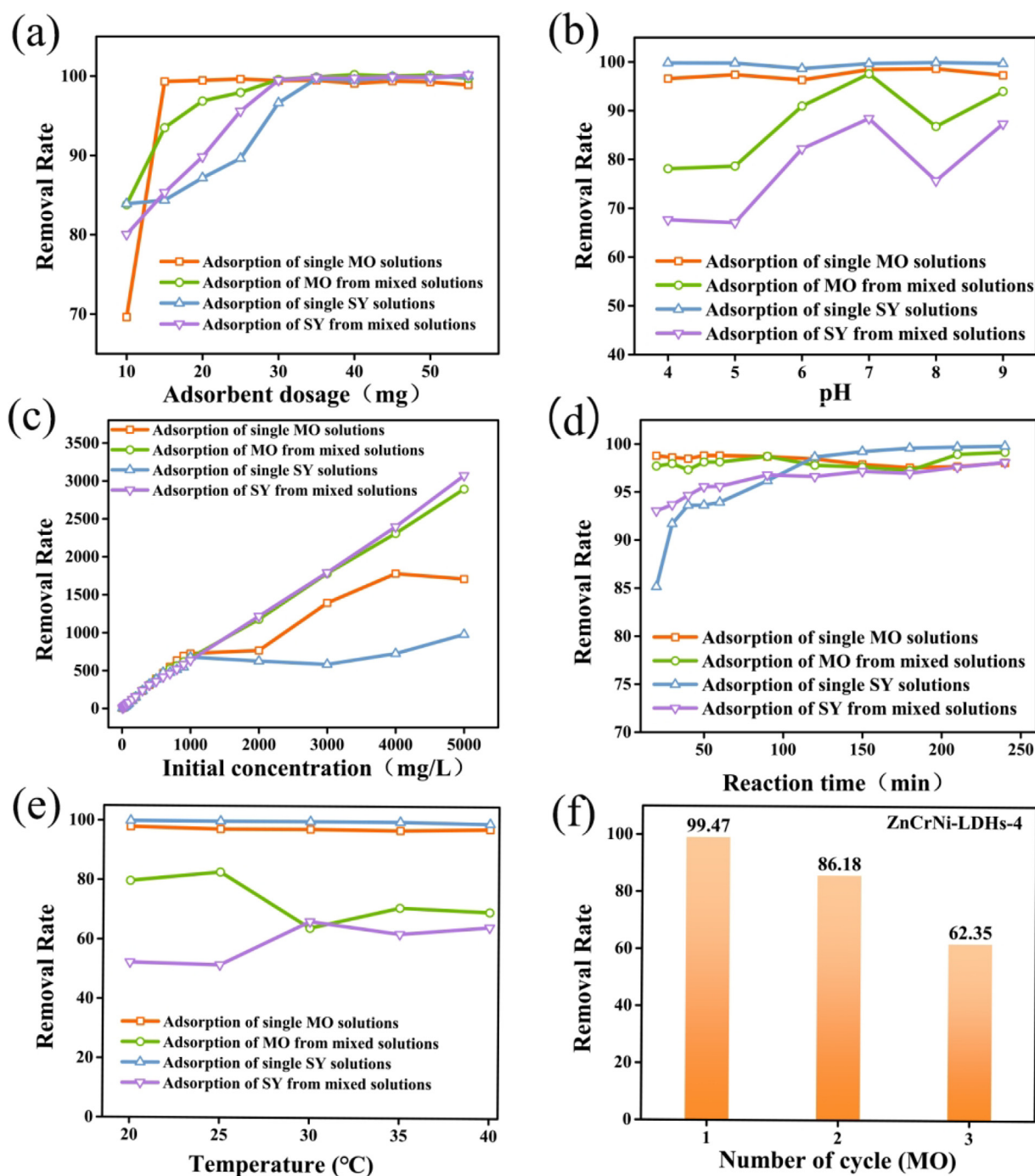


**Fig. 4** Effect of ZnCrNi-LDHs-4 adsorbent dosage (a), pH (b), Effect of initial concentration (c), adsorption time (d), adsorption temperature (e) and cycling performance tests (f) on single and mixed solutions.

bent on the single solution is worse than the adsorption of the mixed solution in the high concentration range (2000 mg/L-5000 mg/L). The increase in solute increases the concentration gradient of the solution and speeds up the movement of the particles, while the molecular chain lengths of MO and SY are different, the 3D stacked gradation porous nanomaterials were more dispersed in the mixed solution during the adsorption process, storming more adsorption sites and thus allowing more anions to be adsorbed.

Fig. 4(d) illustrates the impact of adsorption time from 0 to 240 min on the adsorption performance of adsorbed single and mixed solutions. The removal rate of single MO/SY increased sharply in short time and raised a maximum value at 10 min for the availability of free active sites of the ZnCrNi-LDHs, then reached a stable platform. Overall, the adsorption time had little effect on the adsorption performance of the adsorbed single and mixed solutions, but it was evident that the removal rate of the adsorbed single solution by the adsorbent was

higher than the adsorption rate of the mixed solution. The adsorption of MO and SY in the mixed solution was still increasing, indicating that the layer spacing of ZnCrNi-LDHs becomes larger due to the ion exchange of large pollutants like MO and SY with nitrate ions, which is more conducive to the entry of anionic pollutants and the output of nitrate ions, thus improving the adsorption capacity of the adsorbent and also reflecting the synergistic removal of MO and SY. The max adsorption capacities are 1834.63 and 1259.79  $\text{mg}\cdot\text{g}^{-1}$  for MO and SY, respectively. Table 2 shows the maximum adsorption capacities of ZnCrNi-LDHs-4 and other LDH adsorbents for MO and SY. Comparing to the maximum adsorption capacities of other adsorbents reported toward MO and SY adsorption, the adsorption capacity is superior to some adsorbents such as Zn-Fe-NO<sub>3</sub>-LDH, ZnAl-Cl-LDH@Al(OH)<sub>3</sub>, ZnMgAl-LDH, LDH-S. etc, so ZnCrNi-LDHs-4 can be considered to be excellent candidate for the remove of MO and SY from waste water.

### 3.2.3. The effect of adsorption temperature on the adsorption of MO/SY mixed solution and regeneration

Fig. 4(e) represents the impact of adsorption temperature on the adsorption performance of adsorbing single and mixed solutions. Under the fixed conditions of pH, adsorbent dosage, volume, initial concentration of MO/SY and stirring rate, the temperature of the methyl orange/sunset yellow solution was varied from 20 °C to 40 °C and stirred for 1 h. The remaining concentration of MO/SY was measured respectively after the adsorption was completed and the equilibrium adsorption amount was calculated. It can be seen from Fig. 4(a) that the higher removal rate for the single solution than that of the

mixed solution. The reason is that the adsorbent is quantitative and can provide a limited adsorption sites number, so it leads to a lower overall removal rate for more solutes in the mixed solution. In the mixed solution, the molecular movement is stronger and the disorder of the system increase as the temperature increases from 25 °C to 30 °C, the SY removal increases. This phenomenon corresponds to the synergistic removal effect of MO and SY.

Fig. 4(f) Regeneration tests were carried out using the recovery of the adsorbent ZnCrNi-LDHs-4 to explore the potential utilization of hydrotalcite. Three cycles of experiments were carried out using MO as the mock dye with removal rates of 99.47%, 86.18% and 62.35% respectively. The results showed that most of the adsorption sites could be recovered using adsorption-desorption and that the adsorbent is a promising hydrotalcite-like material for the application.

### 3.2.4. Adsorption isotherms of mixed MO/SY solutions

Adsorption isotherms provide qualitative information on the capacity of the adsorbent and the nature of the solute-surface interaction. The adsorption isotherm was fitted using the adsorption data by the Langmuir and Freundlich equation. According to the definition of the adsorption isotherm, the Langmuir isotherm is based on the theoretical assumption that the adsorption process occurs at a homogeneous location within the adsorbent and that once an adsorption site is occupied, no adsorption will occur at that site. This suggests that the Langmuir isotherm assumes that the theoretical surface is monolayer adsorbed and that its adsorption results in a saturation value. The Freundlich isotherm fitting equation is an

**Table 2** Compares with the adsorption capacity of MO/SY with other adsorbent materials.

Analyte	Adsorbent	Maximum adsorption capacity ( $Q_m$ , $\text{mg}\cdot\text{g}^{-1}$ )	Adsorption isotherm	References
MO	DI-LDH-Ns	846.6	Langmuir	(Lei et al., 2020)
	NiFe LDH	206	Langmuir	(Lu et al., 2016)
	Zn-Fe-NO <sub>3</sub> -LDH	508.2	Langmuir	(Moustafa et al., 2021)
	NiFe-Cl-LDH	769.2	Langmuir	(Gao et al., 2018)
	ZnAl-Cl-LDH@Al(OH) <sub>3</sub>	1013.5	Langmuir	(Guo et al., 2018)
	ZIF-67@LDH	1029.6	Langmuir	(Saghir and Xiao, 2021)
	MgAl-Cl-LDH	1112	Langmuir	(Xu et al., 2017)
	Co4Fe-NO <sub>3</sub> -LDH	1290	Langmuir	(Ling et al., 2016.A)
	ZnAl-LDO@C	1538.9	Langmuir	(Li et al., 2020)
	ZnMgAl-LDH	883.2	Freundlich	(Zheng et al., 2012)
	MgAl-LDH	377.9	Freundlich	(Ping et al., 2018)
	Starch-NiFe-LDH	388	Freundlich	(Zubair et al., 2017)
	LDH-S	1250	Freundlich	(Ko et al., 2021)
	ZnCrNi-LDHs-4	1834.63	Freundlich	this work
SY	Cu-ZnS-AC	85.397	Langmuir	(Agarwal et al., 2016)
	Biochars	74.07	Langmuir	(Mahmoud et al., 2020)
	Neodymium-embedded ordered mesoporous carbon	285.7	Langmuir	(Ahmad et al., 2019)
	Mn-Fe LDH/CS fibers	11.37	Langmuir	(Khalili et al., 2021)
	Chitosan	611.27	Freundlich	(Lei et al., 2020)
	Chitosan-APTES	95	Freundlich	(Lima et al., 2019)
	ZnCrNi-LDHs-4	1259.79	Freundlich	this work

**Table 3** Isotherm fitting parameters for the adsorption of methyl orange (MO) and sunset yellow (SY) by ZnCrNi-LDHs-4.

Adsorption solution		Langmuir equation			Freundlich equation		
		$Q_m(\text{mg}\cdot\text{g}^{-1})$	$R_L$	$R^2$	$n$	$R_F$	$R^2$
MO		3365.768	0.0002286	0.7332	1.07	0.9600	0.98168
SY		1104.384	0.0007002	0.8499	1.16	1.1672	0.9326
Mixed solutions	MO	11265.105	0.0000654	0.6288	1.03	0.8039	0.99701
	SY	9900.500	0.0000777	0.6370	1.06	1.0164	0.99885

**Table 4** Kinetic fitting parameters for the adsorption of methyl orange (MO) and sunset yellow (SY) by ZnCrNi-LDHs.

Adsorption solution		Pseudo first-order			Pseudo second-order		
		$Q_e$	$K_1$	$R^2$	$Q_e$	$K_2$	$R^2$
MO		0.762997	-0.0076	0.1660	389.1050	-0.007266	0.99997
SY		5.332445	0.00205	0.0075	487.805	7.881E-07	0.99006
Mixed solutions	MO	4.587521	-0.0040	0.0513	386.100	-0.014463	0.99994
	SY	9.207515	0.00554	0.0962	364.9635	0.0429513	0.99963

empirical equation that assumes that adsorption occurs on a multiphase surface of the adsorbent and that the amount of adsorbed material is influenced by the initial concentration of the adsorbate. As can be seen in Table 3, the adsorption process more fits the Freundlich model than Langmuir model. The  $n$  values of ZnCrNi-LDHs-4 for the adsorption of MO, SY and mixed solutions in Table 2 are all greater than 1, indicating that ZnCrNi-LDHs-4 is a favorable process for the adsorption of MO/SY (Chakraborty and Acharya, 2018).

### 3.2.5. Adsorption kinetics of ZnCrNi-LDHs on mixed MO/SY solutions

As can be seen in Table 4, the adsorption process fits in the pseudo-secondary kinetic model and the  $R^2$  values of the correlation coefficients fitted by the pseudo-secondary kinetics are higher than the  $R^2$  values of the pseudo-firsties, indicating that the adsorption of the products to MO follows the pseudo-secondary kinetic model. The adsorption process may be controlled by chemisorption or chemical bonding between the active sites of the adsorbent (Behbahani et al., 2020). The theoretical adsorption of the single solution adsorption fit matched the actual adsorption and the adsorbent adsorption of methyl orange was superior to that of sunset yellow.

### 3.2.6. Thermodynamics of adsorption of mixed MO/SY solutions

The temperature influence on the adsorption of MO/SY and mixed MO/SY solutions by ZnCrNi-LDHs-4 were evaluated at 293, 298, 303, 308 and 313 K. The thermodynamic parameters such as the enthalpy change( $\Delta H$ ), entropy change( $\Delta S$ ) and Gibbs free energy( $\Delta G$ ) were calculated by the following equations (Bharali and Deka, 2017):

$$\ln K_d = \frac{S}{R} - \frac{H}{RT} \quad (3)$$

$$\Delta G = -RT \ln K_d \quad (4)$$

Where  $K_d = q_e/C_e$ ,  $T$  and  $R$  are the thermodynamic equilibrium constant(L/g), the absolute temperature (K) and the universal gas constant (8.314 J/mol K), respectively.  $\Delta H$  and  $\Delta S$  can be calculated through the slope and intercept of the plot of  $\ln K_d$  versus  $1/T$ .

As shown in Table 5, the thermodynamic calculations revealed that the enthalpy change  $\Delta H$  greater than 0 for the adsorption process of Zn-Cr-Ni-LDHs-4 on MO, SY and mixed MO and SY which indicated that the adsorption process was a heat absorption process, and the entropy change  $\Delta S$  greater than 0 indicates that the disorder in the adsorption process of MO, SY and mixed MO and SY increases, the system increases in disorder with increasing temperature, and the Gibbs free energy  $\Delta G$  less than 0 indicate that the adsorption process of MO/SY onto Zn-Cr-Ni-LDHs-4 was spontaneous through thermodynamic calculations. It can also be seen that the values of  $\Delta G$  ( $\Delta G < -20$  KJ/mol) which show that adsorption is physical adsorption process. As we all know, the adsorption potential  $E < 8$  KJ/mol or  $E > 8$  KJ/mol, the adsorption process is physical adsorption or ion exchange adsorption (El Hassani et al., 2017), respectively. As shown in Table 5, the values of  $E$  are between 0 and  $-20$  KJ/mol which show that this adsorption process exist physical adsorption and ion exchange adsorption.

### 3.2.7. Adsorption mechanisms

In general, the adsorption of dye molecules mainly depends on electrostatic attraction and ion exchange by the interlayer  $\text{OH}^-$  and  $\text{NO}_3^-$  using LDHs as adsorbent (Remediation, 2022). In this paper, the adsorption mechanism was further explored to understand the adsorption separation process for MO/SY and mixed MO/SY solution using ZnCrNi-LDHs-4 as adsorbent by FTIR spectrum, SEM and XRD patterns.

The XRD results of ZnCrNi-LDHs-4 before and after MO/SY adsorption are shown in Fig. 5. As illustrated in Fig. 5a, it can be seen that the layer spacing becomes larger and the diffraction angle decreases accordingly. The (003) peak is

Adsorption solution	T/K	C <sub>0</sub> /(mg/L)	C <sub>e</sub> /(mg/L)	E (KJ/mol)	ΔG (KJ/mol)	ΔH (KJ/mol)	ΔS [KJ·(mol·K) <sup>-1</sup> ]	
MO	293	500	10.40	9.43	-2.65	0.22	8.91	
	298		14.28	8.81	-2.62			
	303		14.06	9.00	-2.77			
	308		15.50	8.90	-3.28			
	313		13.23	9.45	-2.69			
SY	293	500	0.49	16.85	-2.77	0.21	9.64	
	298		1.08	15.21	-2.50			
	303		0.93	15.83	-2.63			
	308		1.25	15.35	-2.70			
	313		3.86	12.66	-2.82			
Mixed solutions	MO	500	101.38	3.89	-2.61	6.58	8.55	
			298	86.74	4.34			-2.83
			303	180.21	2.57			-2.50
			308	145.74	3.16			-2.59
			313	152.34	3.09			-2.66
	SY	500	238.85	1.80	-2.73	9.31	8.82	
			298	242.92	1.79			-2.79
			303	169.11	2.73			-3.02
			308	189.95	2.48			-2.67
			313	177.81	2.69			-2.77

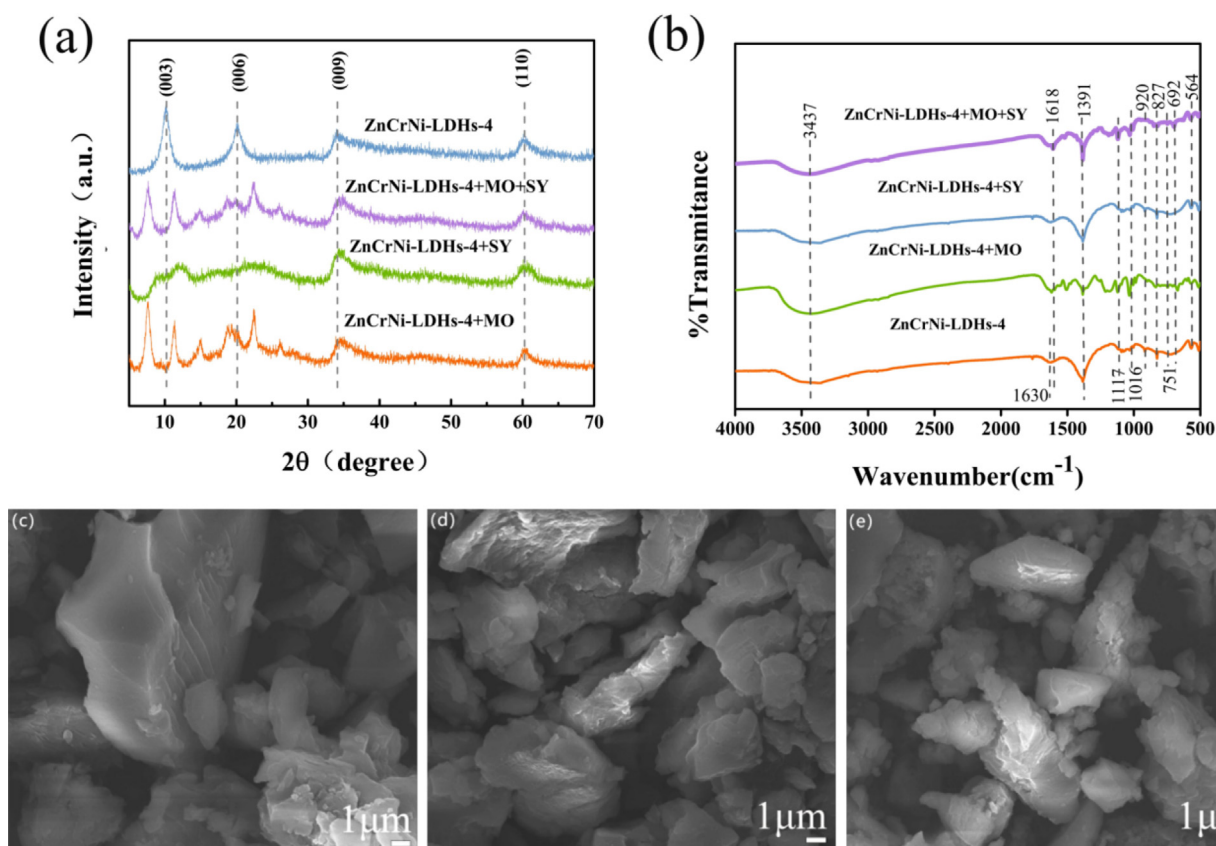


**Fig. 5** XRD pattern (a), FTIR pattern (b) and SEM (c-e) of adsorbed MO/SY with ZnCrNi-LDHs.

shifted from 10.28 to 7.69° ( $\Delta = 2.59^\circ$ ) for ZnCrNi-LDHs-4 which is due to the increasing of the spacing of layers from 0.860 to 1.149 nm because of the exchange of anions, indicating that the interlayer space of ZnCrNi-LDHs-4 after MO and

mixed MO/SY adsorption significantly increased because of slantly between the layers (Enyi, 2022), this results is consistent with the structure analysis of SEM. While, comparing to that of before and after MO adsorption, XRD curves before and

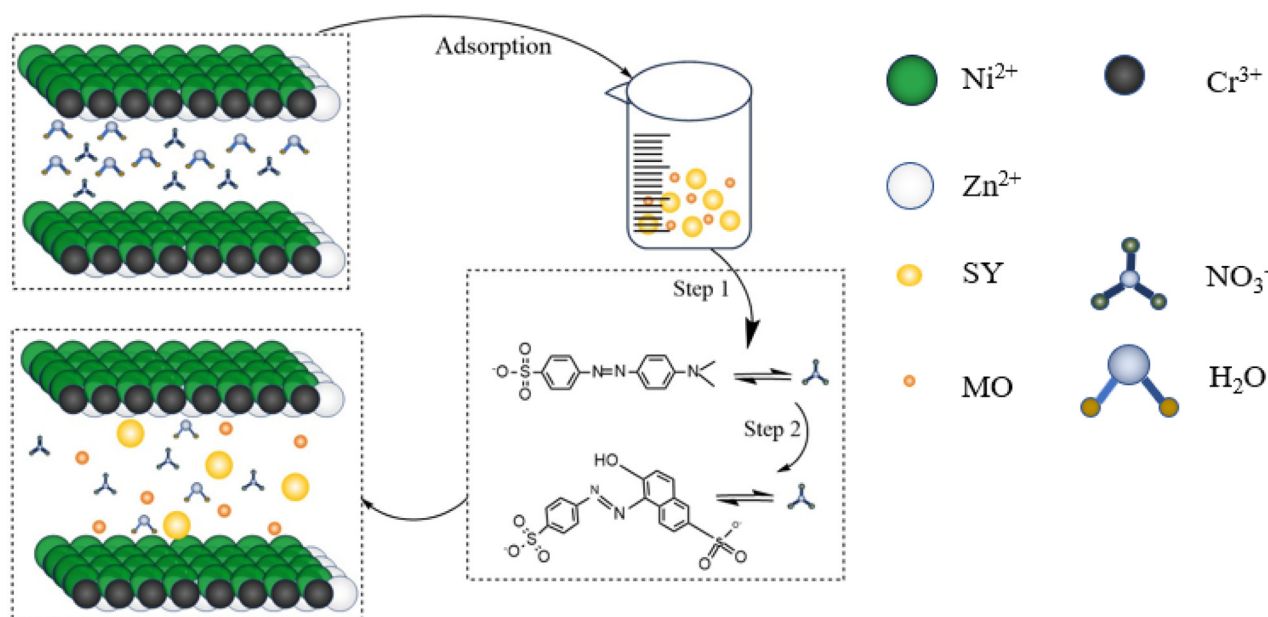


Fig. 6 Illustration of adsorption of ZnCrNi-LDHs.

after SY adsorption for ZnCrNi-LDHs-4 disappear, indicating the relatively large molecular size of SY is not conducive to entering the interlayer structure of LDH from the adsorption solution and finally destroys the well-ordered ZnCrNi-LDHs-4 structure (Jie, 2022). Meanwhile; it can also be seen that the XRD curves of the mixed solution after adsorption nearly identical to that of before MO adsorption through ion exchange, van der Waals forces and electrostatic attraction with further adsorption, indicating the adsorption of MO and SY did not destroy the well-ordered LDH structure. This phenomenon shows that the adsorption process is completed in stages according to the molecular size and larger radius from small to large in mixed solution. It is note that the intensity of the diffraction peak decrease from after MO/SY to mixed MO/SY adsorption, indicating that the crystallinity of the material becomes lower because the more anions from the adsorption solution have successfully entered the interlayer. To determine whether the substances making the interlayer spacing larger were MO and SY, another means of characterizing the residues after adsorption was carried out.

Fig. 5(b) shows the IR spectra of the Zn-Cr-Ni-LDHs after the adsorption of MO and SY. The absorption peak at  $1618\text{ cm}^{-1}$  is attributed to the stretching vibration of the aromatic C-C, The absorption peak at  $1391\text{ cm}^{-1}$  is attributed to the N = N peak in MO and SY, and the peaks at  $1117\text{ cm}^{-1}$  and  $1016\text{ cm}^{-1}$  are associated with the sulfonic acid group ( $-\text{SO}_3$ ) about S = O bond stretching vibrations (Ahmed and Gasser, 2012); The skeletal vibrations of the aromatic rings for asymmetric and symmetric vibration of MO and SY were confirmed by the vibration bands at  $1608\text{--}1442\text{ cm}^{-1}$  region. The peaks at  $920\text{ cm}^{-1}$ ,  $827\text{ cm}^{-1}$ ,  $751\text{ cm}^{-1}$ ,  $692\text{ cm}^{-1}$  are attributed to C-H stretching vibrations in the aromatic atomic nuclei related to out-of-plane bending vibrations (Zheng et al., 2017), confirming the entry of MO and SY molecules into the interlayer of the Zn-Cr-Ni-LDHs-4.

The SEM of Zn-Cr-Ni-LDHs-4 adsorbed MO/SY are shown in Fig. 5 (c-e). Based on the comparison of SEM before

and after MO/SY adsorption, it can be seen that the 3D stacked lamellar structures become dispersed due to the insertion of dye anions, and the larger layer spacing exposes more active sites between the layers, which is more conducive to the adsorption for dye anions, which is consistent with the smaller diffraction angle and larger layer spacing in XRD (Yishang, 2018). Meanwhile, the charge value of the surface of ZnCrNi-LDHs-4 was determined to be positive by Zeta potential analysis, and there was also surface adsorption during the adsorption process for MO/SY, and MO and SY were also partly adsorbed on the surface of the nanosheets. In conclusion, the rapid high adsorption process is dominated by surface adsorption and interlayer ion exchange. ZnCrNi-LDHs-4 containing mesoporous and macroporous are also more favorable for the entry of MO and SY molecules.

Based on the above analysis the following adsorption, a possible adsorption mechanism will be proposed as shown in Fig. 6. In this paper, methyl orange molecules are shorter than sunset yellow, ZnCrNi-LDHs-4 first adsorbs methyl orange molecules with short molecular chain length, and  $\text{OH}^-$  and  $\text{NO}_3^-$  are replaced by methyl orange molecules in the form of ion exchange. The entry of methyl orange molecules makes the nanosheets disperse and the layer spacing between the nanosheets becomes larger, and then sunset yellow also enters the interlayer by ion exchange. There are more active site leaks between irregularly stacked layers, which can allow more methyl orange and sunset yellow molecules to enter the layers by ion exchange.

#### 4. Conclusion

In this study, ZnCrNi-LDHs were prepared for the adsorption of methyl orange, sunset yellow, and mixed solutions using the hydrothermal method. ZnCrNi-LDHs-4 showed superior adsorption capacity than ZnCrNi-LDHs-2 and ZnCrNi-LDHs-3. There are ion exchange process and electrostatic attraction in the adsorption process according to the SEM, IR, zeta potential and XRD before and after

adsorption. The adsorption of methyl orange, sunset yellow, and mixed solutions in ZnCrNi-LDHs-4 followed a quasi-secondary kinetic model, and the adsorption process belonged to multilayer adsorption. The adsorption isotherms of all three ZnCrNi-LDHs follow the Freundlich model, and there is chemisorption for the adsorption process. The adsorption thermodynamics indicated that the adsorption process is a heat absorption reaction that proceeds spontaneously. Therefore, the hierarchical porous structure of the material and the positive charge on the surface conferred excellent adsorption properties to the material itself, and the synergistic effect of methyl orange and sunset yellow also contributed to the enhanced adsorption capacity. The maximum adsorption capacity could reach 1834.63 mg/g, 1259.79 mg/g, 3270.59 mg/g, and 3294.38 mg/g, respectively. In addition, the regeneration experiments proved that ZnCrNi-LDHs maintained a removal rate of 62.35% for three cycles, which can be used as a potential adsorbent, and the subsequent adsorption enrichment and then photocatalytic degradation can be used to improve the reusability of this adsorbent as well as the complete mineralization of the adsorbed pollutants. This result not only demonstrates that the three ZnCrNi-LDHs materials exhibit excellent adsorption performance and practical significance as efficient adsorbents for the removal of MO, SY, and mixed solutions, but also provides a strategy for the removal of mixed dye solutions.

### Funding

This work was supported by the National Natural Science Foundation of China (21771165), Provincial Key Technologies R & D Program of Henan (192102310237, 172102310556) and the Key Program of the Henan universities and colleges (20B150031, 19A140018).

### CRedit authorship contribution statement

**Li Yang:** Investigation, Formal analysis. **Tian Huiyuan:** . **Xia Mengyan:** . **Cui Baoyu:** . **Liu Chang:** . **Du Xiuhong:** . **Wang Zehua:** . **Duan Xianying:** Supervision. **Cui Jiehu:** Conceptualization, Methodology, Supervision, Funding acquisition.

### Declaration of Competing Interest

The authors declare that they have no known competing financial interests or personal relationships that could have appeared to influence the work reported in this paper.

### References

- Ibrahim Abdelfattah, Fathy A. El-Saied, Ali A. Almedolab, A.M. El-Shamy, 2022. Biosorption as a Perfect Technique for Purification of Wastewater Contaminated with Ammonia. *Appl Biochem Biotech.* 194:4105–4134. DOI:10.1007/s12010-021-03794-4.
- Agarwal, S., Tyagi, I., Gupta, V.K., Dastkhon, M., Ghaedi, M., Yousefi, F., Asfaram, A., 2016. Ultrasound-assisted adsorption of Sunset Yellow CFC dye onto Cu doped ZnS nanoparticles loaded on activated carbon using response surface methodology based on central composite design. *J. Mol. Liq.* 219, 332–340. <https://doi.org/10.1016/j.molliq.2016.02.100>.
- Ahmad, Z.U., Yao, L., Wang, J., Gang, D.D., Islam, F., Lian, Q., Zappi, M.E., 2019. Neodymium embedded ordered mesoporous carbon (OMC) for enhanced adsorption of sunset yellow: Characterizations, adsorption study and adsorption mechanism. *Chem. Eng. J.* 359, 814–826. <https://doi.org/10.1016/j.cej.2018.11.174>.
- Ahmed, I.M., Gasser, M.S., 2012. Adsorption study of anionic reactive dye from aqueous solution to Mg-Fe-CO<sub>3</sub> layered double hydroxide (LDH). *Appl. Surf. Sci.* 259, 650–656. <https://doi.org/10.1016/j.apsusc.2012.07.092>.
- Elham Sadati Behbahani, Kheibar Dashtian, Mehrorang Ghaedi, 2020. Fe<sub>3</sub>O<sub>4</sub>-FeMoS<sub>4</sub>: promise magnetite LDH-based adsorbent for simultaneous removal of Pb (II), Cd (II), and Cu (II) heavy metal ions. *J. Haz. Mat.* 410:124560.1-124560.11. DOI: 10.1016/j.jhazmat.2020.124560.
- Bharali D, Deka R C, 2017. Preferential adsorption of various anionic and cationic dyes from aqueous solution over ternary CuMgAl layered double hydroxide[J]. *Colloid Surface A.* 525:64-76. DOI: 10.1016/j.colsurfa.2017.04.060.
- Chakraborty, A., Acharya, H., 2018. Facile synthesis of MgAl-layered double hydroxide supported metal organic framework nanocomposite for adsorptive removal of methyl orange dye. *Colloid. Interface Sci.* 24, 35–39. <https://doi.org/10.1016/j.colcom.2018.03.005>.
- Chen, Z.J., Guo, H., Liu, H.Y., et al, 2022. Construction of dual S-scheme Ag<sub>2</sub>CO<sub>3</sub>/Bi<sub>4</sub>O<sub>5</sub>I<sub>2</sub>/g-C<sub>3</sub>N<sub>4</sub> heterostructure photocatalyst with enhanced visible-light photocatalytic degradation for tetracycline. *Chem. Eng. J.* 2022, (438). <https://doi.org/10.1016/j.cej.135471> 135471.
- Chen, Y., Jing, C., Zhang, X., et al, 2019. Acid-salt treated CoAl layered double hydroxide nanosheets with enhanced adsorption capacity of methyl orange dye. *J. Colloid Interface Sci.* 548, 100–109. <https://doi.org/10.1016/j.jcis.2019.03.107>.
- Chen, R., Yu, J., Xiao, W., 2013. Hierarchically porous MnO<sub>2</sub> microspheres with enhanced adsorption performance. *J. Mater. Chem. A* 1 (38), 11682–11690. <https://doi.org/10.1039/C3TA12589K>.
- Chen, H., Zhang, H., Zhou, X., et al, 2021. Study on the adsorption performance of modified activated carbon for methylene blue and Cd<sup>2+</sup> complex. *Appl. Chem. Indus.* 50 (10), 2699–2705. <https://doi.org/10.1021/acscenergylett.9b02280>.
- Cheng, Y.a., 2012. Preparation of hierarchically porous layered double hydroxides and their adsorption performance [D]. *Wuhan University of Technology*.
- Cui J, Wei C, Zhang M, et al, 2020. 2D to 3D controllable synthesis of three Zn-Co-LDHs for rapid adsorption of MO by TEA-assisted hydrothermal method[J]. *Appl. Surf. Sci.* 534(8): 147564. DOI: 10.1016/j.apsusc.2020.147564.
- Dong, Z., Bi, J., Hai, B., 2017. Preparation of nickel-cobalt-chromium ternary hydroxalcite and its electrochemical properties [J]. *Technol. Develop. Chem. Indus.* 46 (9), 4.
- Dong C, Yuan X, Wang X, et al, 2016. Rational design of cobalt-chromium layer double hydroxide as a highly efficient electrocatalyst for water oxidation[J]. *J. mater. chem. a.* 4:11292-11298. DOI:10.1039/C6TA04052G.
- Duan G, Cai W, Luo Y, et al, 2010. A Hierarchically Structured Ni (OH)<sub>2</sub> Monolayer Hollow-Sphere Array and Its Tunable Optical Properties over a Large Region[J]. *Adv. Funct. Mater.* 17(4):644-650. DOI:10.1002/adfm.200600568.
- El Hassani, K., Beakou, B.H., Kalnina, D., Oukani, E., Anouar, A., 2017. Effect of morphological properties of layered double hydroxides on adsorption of azo dye methyl orange: a comparative study. *Appl. Clay Sci.* 140, 124–131. <https://doi.org/10.1016/j.clay.2017.02.010>.
- Environmental Remediation of Contaminated Wastewater with Ammonium Using Clay-Based Adsorbents. DOI:10.46488/NEPT.2022.v2i104.052.
- Enyi, X., 2022. Fabrication of three-dimensional stacked silicon-nanosheet biosensors [D]. *North China University of Technology*.
- Gao, J., Lu, Y., Fang, L., et al, 2018. Efficient removal of methyl orange and heavy metal ion from aqueous solution by NiFe-Cl-layered double hydroxide. *Environ. Eng. Sci.* 35, 373–381. <https://doi.org/10.1089/ees.2017.0023>.
- Ghaedi, M., Mohammadi, F., Ansari, A., 2015. Gold nanoparticles loaded on activated carbon as novel adsorbent for kinetic and isotherm studies of methyl orange and sunset yellow adsorption. *J.*

- Disper. Sci. Technol. 36 (5), 652–659. <https://doi.org/10.1080/01932691.2014.893527>.
- Grover, A., Mohiuddin, I., Malik, A.K., et al, 2022. Magnesium/aluminum layered double hydroxides intercalated with starch for effective adsorptive removal of anionic dyes. *J. Hazard. Mater.* 424. <https://doi.org/10.1016/j.jhazmat.2021.127454> 127454.
- Guo, X., Yin, P., Yang, H., 2018. Superb adsorption of organic dyes from aqueous solution on hierarchically porous composites constructed by ZnAl-LDH/Al(OH)<sub>3</sub> nanosheets. *Micropor. Mesopor. Mat.* 259, 123–133. <https://doi.org/10.1016/j.micromeso.2017.10.003>.
- Hucheng Fu, Aitang Zhang, Hanwen Guo, Hanwen Zong, Fuhao Jin, Kai Zhao, Jingquan Liu, 2022. Rose-like ZnNiCo layered double hydroxide grown on Co<sub>3</sub>O<sub>4</sub> nanowire arrays for high energy density flexible supercapacitors. *J. Energy Storage*.56, 106056. DOI: 10.1016/j.est.2022.106056.
- Ji, Z., Hou, G., Wang, J., et al, 2009. The effect of the specific surface area and pore radius distribution of inorganic materials on the capacity of absorbing and desorbing moisture in the air. *Acta Petrol. Mineral.* 28 (06), 653–660. <https://doi.org/10.1109/MILCOM.2009.5379889>.
- Jiang, Z., Sun, F., Frost, R.L., et al, 2022. Adsorption characteristics of assembled and unassembled Ni/Cr layered double hydroxides towards methyl orange. *J. Colloid Interface Sci.* 617, 363–371. <https://doi.org/10.1016/j.jcis.2022.03.022>.
- Jie, Z.u., 2022. LDHs and their nanocomposites for adsorption/photocatalysis of degradation dye wastewater [D]. Zhengzhou University of Aeronautics.
- Jie, Z., Yichen, J., Ping, L., et al, 2022. Rational construction and understanding the effect of metal cation substitution of three novel ternary Zn-Co-Ni-LDHs from 2D to 3D and its enhanced adsorption properties for MO. *Environ. Sci. Pollut. R.* 1–19. <https://doi.org/10.1007/s11356-022-22303-6>.
- Khalili, R., Ghaedi, M., Parvinnia, M., Sabzehmeidani, M.M., 2021. Simultaneous removal of binary mixture dyes using mn-Fe layered double hydroxide coated chitosan fibers prepared by wet spinning. *Surf. Interfaces* 23. <https://doi.org/10.1016/j.surfin.2021.100976> 100976.
- Ko, S.J., Yamaguchi, T., Salles, F., et al, 2021. Systematic utilization of layered double hydroxide nanosheets for effective removal of methyl orange from an aqueous system by  $\pi$ - $\pi$  stacking-induced nanoconfinement. *J. Environ. Manage.* 277. <https://doi.org/10.1016/j.jenvman.2020.111455> 111455.
- Lei, Z.A., Ls, B., Df, C., et al, 2020. Adsorption of dyes brilliant blue, sunset yellow and tartrazine from aqueous solution on chitosan: Analytical interpretation via multilayer statistical physics model - ScienceDirect[J]. *Chem. Eng. J.* 382. <https://doi.org/10.1016/j.cej.2019.122952> 122952.
- Lei, S., Wang, S., Gao, B., et al, 2020. Ultrathin dodecyl-sulfate-intercalated Mg-Al layered double hydroxide nanosheets with high adsorption capability for dye pollution. *J. Colloid Interface Sci.* 577 (1), 181–190. <https://doi.org/10.1016/j.jcis.2020.05.050>.
- Lei, C., Zhu, X., Yao, L., et al, 2016. Hierarchically porous NiO-Al<sub>2</sub>O<sub>3</sub> nanocomposite with enhanced Congo red adsorption in water. *RSC Adv.* 6 (13), 10272–10279. <https://doi.org/10.1039/c5ra23545f>.
- Lei, C., Pi, M., Jiang, C., et al, 2017. Synthesis of hierarchical porous zinc oxide (ZnO) microspheres with highly efficient adsorption of Congo red. *J. Colloid & Interface Sci.* 490, 242–251. <https://doi.org/10.1016/j.jcis.2016.11.049>.
- Li, M., Wu, G., Liu, Z., et al, 2020. Uniformly coating ZnAl layered double oxide nanosheets with ultra-thin carbon by ligand and phase transformation for enhanced adsorption of anionic pollutants. *J. Haz. Mat.* 397. <https://doi.org/10.1016/j.jhazmat.2020.122766> 122766.
- V.V.C. Lima, F.B. Dalla Nora, E.C. Peres, G.S. Reis, E.C. Lima, M. L.S. Oliveira, G. L. Dotto, 2019. Synthesis and characterization of biopolymers functionalized with APTES (3-aminopropyltriethoxysilane) for the adsorption of sunset yellow dye. *J. Environ. Chem. Eng.* 7, 103410. DOI: 10.1016/j.jece.2019.103410.
- Lin J, Zhang Y, Zhang Q, et al, 2022. Study on adsorption and photocatalytic regeneration capability of Zn<sub>3</sub>Cr-CO<sub>3</sub> LDH as adsorbent for removal of methyl orange. *Journal of Henan Polytechnic University: natural science*.41(5):9. DOI: 10.3321/j.issn:0253-2417.2005.03.010.
- Lin J, Zhang Y, Zhang Q, et al, 2021. Enhanced adsorption properties of organic ZnCr-LDH synthesized by soft template method for anionic dyes. *Environ. Sci. Pollut. R.*, 1-17. DOI:10.1007/s11356-021-14035-w.
- Ling, F., Fang, L., Lu, Y., et al, 2016. A novel CoFe layered double hydroxides adsorbent: High adsorption amount for methyl orange dye and fast removal of Cr(VI)[J]. *Micropor. Mesopor. Mat.*, 230–238 <https://doi.org/10.1016/j.micromeso.2016.07.015>.
- Lu, Y., Jiang, B., Fang, L., et al, 2016. High performance NiFe layered double hydroxide for methyl orange dye and Cr(VI) adsorption. *Chemosphere* 152, 415–422. <https://doi.org/10.1016/j.chemosphere.2016.03.015>.
- Lv X Y, Jiang C Y, Ding Y F, et al, 2020. Preparation of Ni (Zn)Cr-LDH/LDO coated magnetic-graphene composites using simulative electroplating wastewaters for oxygen evolution reaction. *Colloid Surface A*.611(1-2): 125839. DOI: 10.1016/j.colsurfa.2020.125839
- Mahmoud, M.E., Abdelfattah, A.M., Tharwat, R.M., et al, 2020. Adsorption of negatively charged food tartrazine and sunset yellow dyes onto positively charged triethylenetetramine biochar: Optimization, kinetics and thermodynamic study. *J. Mol. Liq.* 318. <https://doi.org/10.1016/j.molliq.2020.114297> 114297.
- Mitani, Y., Takei, T., Yanagida, S., et al, 2017. Hybridization of Ni-Cr, Cu-Cr, and Zn-Cr layered double hydroxides with polyoxometalates and their catalytic behavior. *J. Cera. Soc. Jpn.* 125 (10), 747–752. <https://doi.org/10.2109/jcersj2.17060>.
- Moustafa, D., Mahmoud, R., El-Salam, H.M.A., et al, 2021. Utilization of residual zinc-iron-layered double hydroxide after methyl orange management as a new sorbent for wastewater treatment. *Appl. Nanosci.* 11 (31), 709–723. <https://doi.org/10.1007/s13204-020-01632-3>.
- Ping, Z., Ouyang, S., Peng, L., et al, 2018. Enhanced removal of ionic dyes by hierarchical organic three-dimensional layered double hydroxide prepared via soft-template synthesis with mechanism study. *Chem. Eng. J.* 360, 1137–1149. <https://doi.org/10.1016/j.cej.2018.10.179>.
- A, Reda M. Abdelhameed, E. S. B, and M. A. A. E. G. C, 2021. Boosting the photocatalytic activity of Ti-MOF via emerging with metal phthalocyanine to degrade hazard textile pigments. *J. Alloys Compd.* DOI: 10.1016/j.jallcom.2021.162992.
- Rezvani Z, Foruzin L J, Nejadi K, 2023. Intercalation of Mordant orange I into ZnAl-layered double hydroxide and its dual-color photoluminescence emission. *J. Mol. Struct.*1274:134555. DOI:10.1016/j.jmolstruc.2022.134555.
- Saghir, S., Xiao, Z., 2021. Hierarchical mesoporous ZIF-67@LDH for efficient adsorption of aqueous Methyl Orange and Alizarine Red S [J]. *Powder Technol.* 377, 453–463. <https://doi.org/10.1016/j.powtec.2020.09.006>.
- Shan, X., Song, L., Xing, W., et al, 2012. Effect of nickel-containing layered double hydroxides and cyclophosphazene compound on the thermal stability and flame retardancy of poly (lactic acid). *Ind. Eng. Chem. Res.* 51 (40), 13037–13045. <https://doi.org/10.1021/ie300589p>.
- Shoab M, Mazhar M, Mushtaq A et al, 2016. Terahertz time domain spectroscopy of hydrothermally synthesized boehmite and ammonium dawsonite nanostructures[J]. *Infrared phys. techn.*78:200-208. DOI:10.1016/j.infrared.2016.08.007.
- Song, T., Yan, M., Qian, M., 2018. The enabling role of dealloying in the creation of specific hierarchical porous metal structures-A review. *Corros. Sci.* 134. <https://doi.org/10.1016/j.corsci.2018.02.013>.

- Sun, Y., 2015. Intercalation assembly of hydrotalcite materials and enhanced adsorption performance on phenols [D]. Wuhan University of Technology.
- Sun, M.H., Huang, S.Z., Chen, L.H., et al, 2016. Applications of hierarchically structured porous materials from energy storage and conversion, catalysis, photocatalysis, adsorption, separation, and sensing to biomedicine [J]. *Cheminform* 47 (31). <https://doi.org/10.1002/chin.201631285>.
- W D, Fu Y, Yang J, 2022. Enhanced Fluoride Stabilization by Modified Layered Double Hydroxides for the Remediation of Soil Pollution: Performance and Mechanism. *Water, Air, & Soil Poll.*, 233:471. DOI:10.1007/s11270-022-05938-6.
- Wang, Y., Dai, X., Zhou, Q., Li, K., Feng, L., Liao, W., Yu, Y., Yu, H., Zong, X., Lu, G., 2022. Insights into the role of metal cation substitution on the anionic dye removal performance of CoAl-LDH. *Colloid Surface A* 636,. <https://doi.org/10.1016/j.colsurfa.2021.128139> 128139.
- Wang P, Ding N, Wang Y, et al, 2023. Co-MOF Derived NiCo-LDH Three-Dimensional Nanostructure on Carbon Cloth for High-Performance Supercapacitors. *J. Harbin Institute of Technology (New series)* 1-15. DOI:10.1016/j.carbon.2020.04.084.
- Xu, J., Deng, H., Song, J., et al, 2017. Synthesis of hierarchical flower-like Mg<sub>2</sub>Al-Cl layered double hydroxide in a surfactant-free reverse microemulsion. *J. Colloid Interface Sci.* 505, 816. <https://doi.org/10.1016/j.jcis.2017.06.080>.
- Xu, F., Qi, X.Y., Kong, Q., et al, 2017. Adsorption of sunset yellow by luffa sponge, modified luffa and activated carbon from luffa sponge. *Desalin. Water. Treat.* 96 (NOV.), 86–96. <https://doi.org/10.5004/dwt.2017.20925>.
- Yishang, W.U., 2018. Synthesis and mechanism of highly efficient hydrogen evolution catalysis for water splitting [D]. Central South University of Forestry and Technology.
- Zhang, M., 2019. Study on adsorption/photocatalysis of dyewastewater by LZH and its composites [D]. Zhengzhou Univ. Aeronaut.
- Zhang, W., Dong, T., Cheng, H., et al, 2021. Preparation of composite sludge carbon-based materials by LDHs conditioning and carbonization and its application in the simultaneous removal of dissolved organic matter and phosphate in sewage[J]. *Chemosphere* 270,. <https://doi.org/10.1016/j.chemosphere.2020.129485> 129485.
- Zhang Y X, Hao X D, Wang T, et al, 2014. MnO(x)-modified ZnAl-LDOs as high-performance adsorbent for the removal of methyl orange Dalton. *T.43(18):* 6667-6676. DOI:10.1039/c3dt53597e.
- Zhang, L., Shen, Q., Huang, F., et al, 2023. Electrospinning directly synthesis of 0D/1D CuBi<sub>2</sub>O<sub>4</sub>@WO<sub>3</sub> nanofiber photocatalyst with S-scheme heterojunction. *Appl. Surf. Sci.* 608,. <https://doi.org/10.1016/j.apsusc.2022.155064> 155604.
- Zheng, Y., 2019. Fabrication and Congo Red adsorption performance of hierarchically porous materials [D]. Wuhan University of Technology.
- Zheng, Y.M., Na, L., Zhang, W.D., 2012. Preparation of nanostructured microspheres of Zn–Mg–Al layered double hydroxides with high adsorption property[J]. *Colloids Surfaces A Physicochem. Eng. Asp.* 415, 195–201. <https://doi.org/10.1016/j.colsurfa.2012.10.014>.
- Zheng, Y., Zhu, B., Chen, H.a., You, W., Jiang, C., Jiaguo, Y.u., 2017. Hierarchical flower-like nickel (II) oxide microspheres with high adsorption capacity of Congo red in water. *J. Colloid Interface Sci.* 504, 688–696. <https://doi.org/10.1016/j.jcis.2017.06.014>.
- Zheng, Y., Wang, H., Cheng, B., et al, 2018. Fabrication of hierarchical bristle-grass-like NH<sub>4</sub>Al (OH)<sub>2</sub> CO<sub>3</sub>@Ni (OH)<sub>2</sub> core-shell structure and its enhanced Congo red adsorption performance. *J. Alloys Compd.* 750, 644–654. <https://doi.org/10.1016/j.jallcom.2018.04.050>.
- Zubair M, Jarrah N, Ihsanullah, et al, 2017. Starch-NiFe-layered double hydroxide composites: Efficient removal of methyl orange from aqueous phase. *J. Mol. Liq.* 249: 254-264. DOI: 10.1016/j.molliq.2017.11.022.